The architecture and fine structure of gill filaments in the brown mussel, *Perna perna*

M.A. Gregory* and R.C. George
Electron Microscope Unit* and Department of Zoology, University of Durban-Westville, Private Bag X54001, Durban, 4000, South Africa

T.P. McClurg
CSIR, Division of Water, Environment and Forestry Technology, P.O. Box 17001, Congella, 4013, South Africa

Received 31 July 1996; accepted 20 January 1997

For many years, bivalve molluscs have played a useful role in determining the impact of pollution on marine organisms. In the northern hemisphere, ecologists from countries subscribing to the International Mussel Watch have used toxin-mediated changes in the organs of *Mytilus edulis*, especially in the morphology of gill filaments, to indicate the biotoxicity of marine effluent. *M. edulis* is not indigenous to South African waters. For us to adopt a similar approach on the South African east coast, it is necessary to catalogue both the normal appearance and toxin-mediated changes in our local brown mussel *Perna perna*. In this study, the gill filaments from five healthy, adult brown mussels were studied by light and transmission electron microscopy. Special attention was paid to filament architecture, ennervation of filaments, number and type of cells populating filament epithelia and variations in epithelial cell morphology and cilia ultrastructure. Filament shape was maintained by thickened chitin and strategically placed smooth myocytes. The epithelium was populated with eight morphologically distinctive non-secretory, mucus secreting or sensory cell types in various stages of differentiation. Unmyelinated nerves were situated beneath six cell types. Significant differences in filament architecture and epithelial cell morphology were found between *M. edulis* and *P. perna*. It is hoped that this comprehensive description of normal *P. perna* gill filaments will provide a morphological baseline for local pollution impact studies.

* To whom correspondence should be addressed

Introduction

The marine pollution literature is replete with references to bivalve molluscs, particularly mussels and oysters, as they exhibit many of the characteristics which are widely sought in sentinel organisms. They are hardy, ubiquitous, long-lived and easily sampled. Their sedentary nature means that their geographical relationship to a pollution source can be easily ascertained. Mussels, in particular, are prodigious filter feeders and possess enlarged gills, with which individuals may process up to 3 litres of water each hour (Jones, Richards & Southern 1992). Through this regular, intimate contact with their environment, mussels are capable of accumulating traces of biologically available contaminants over an extended period and thus serve as both integrators and magnifiers. It is not surprising, therefore, that they have become so widely employed in pollution impact assessments (Hietanen, Sunila & Kristoffersson 1988; Anderlini 1990; Higashiyama, Shiraishi, Otsuki & Hashimoto 1991).

Clear evidence of the importance of bivalve molluscs in marine pollution impact assessments lies in the magnitude and longevity of the International Mussel Watch (Goldberg, Bowen, Farrington, Harvey, Martin, Parker, Risebrough, Robertson, Schneider & Gamble 1987; Anon. 1980). This programme, which provides a global framework for monitoring pollution levels, originated in the late 1960s and continues to maintain momentum. Most of the effort has so far been concentrated in Europe and North America, and has principally involved *Mytilus californianus*, *M. edulis* and *M. galloprovincialis*. However interest has recently been increasing in areas such as the Asia-Pacific region, Australia and South America (Tavares, Rocha, Porte, Barcelo & Albaiges 1988; Higashiyama *et al.* 1991; Martin & Richardson 1991; Murray, Richardson & Gibbs 1991; Richardson, Garnham & Fabris 1994; Tanabe 1994) in other mussel genera, including *Perna*. South Africa has never formally adopted a mussel watch programme, but has subscribed to its principles in that bivalve molluscs have been widely used in its national marine pollution surveys (Gardner, Connell, Eagle, Moldan, Oliff, Orren & Watling 1983; Hennig 1985).

While the single most common use of mussels in marine pollution studies has undoubtedly been as bioaccumulators of contaminants and microbes, a number of other applications have been covered. These include a wide range of biochemical and physiological stress indicators such as 'scope for growth' (Anderlini 1990), metallothionein induction (Pavicic, Raspor & Branica 1991), acetylcholine inhibition (Bocquene, Galgani, Burgeot, Le Dean & Truquet 1993), lysosomal membrane stability (Winston, Moore, Straatsburg & Kirchin 1991), mixed function oxidase activity (Narbonne, Garrigues, Ribera, Raoux, Mathieu, Lemaire, Salaun & Lafaurie 1991) and immunocompetence (Coles, Farley & Pipe 1994). In addition, a number of researchers have investigated mutagenic and genotoxic effects (Wrisberg & Rhemrev 1992). Some work has also been done on the histological responses of *Mytilus edulis* to pollution in the northern Baltic Sea (Sunila 1986, 1987, 1988; Hietanen *et al.* 1988). With this article, a first step is taken towards a better understanding of the South African brown mussel, *Perna perna*, in relation to pollution impact assessment. It is founded on the premise that, in order to effectively evaluate the effects of pollution, it is vital to establish a baseline of normal conditions. Since the gills are the primary contact points between mussels and their environment, it was decided that a basic morphological description of normal gill filaments in *Perna perna* would constitute a logical starting point.

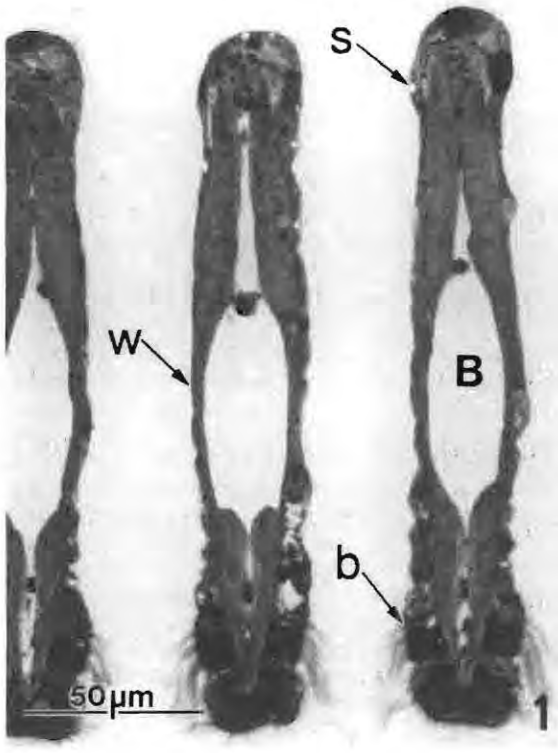

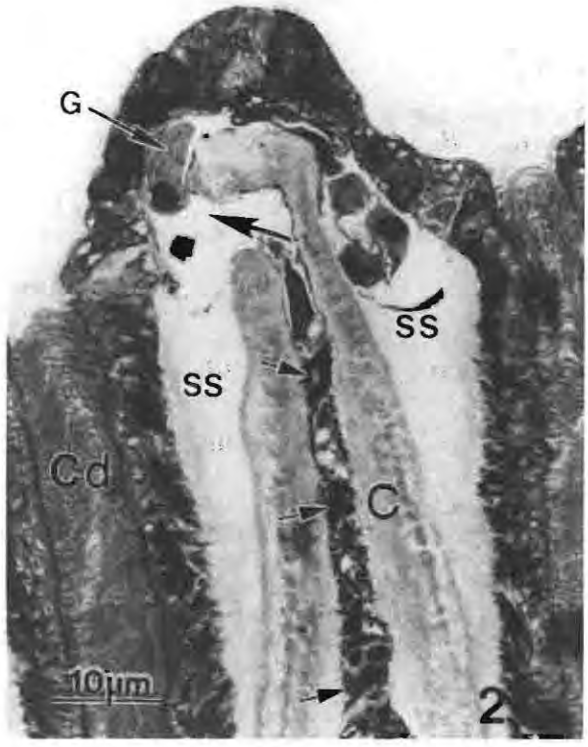

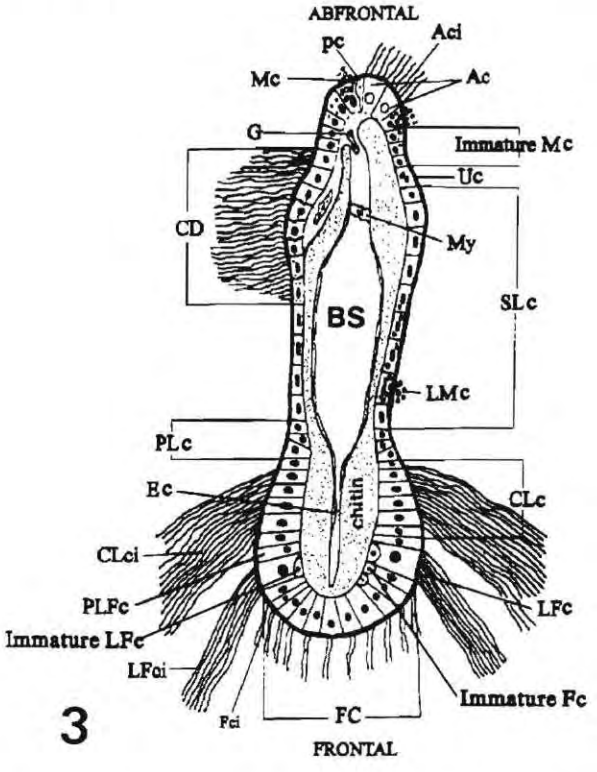

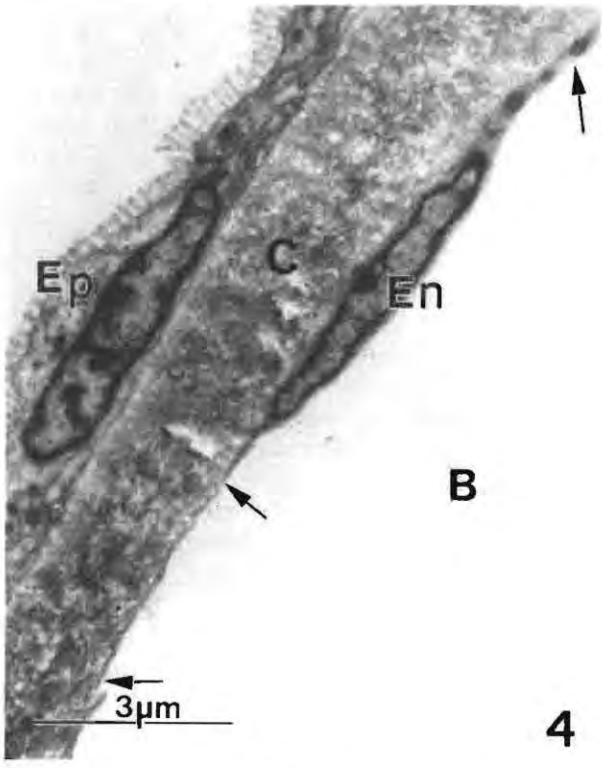

Figure 1 Light micrograph of transversely sectioned filaments in a single lamellum. b = frontal 'bulge'; B = branchial sinus; s = abfrontal 'shoulder'; w = mid-filament 'waist'.

Figure 2 Light micrograph of abfrontal region of transversely sectioned filaments at ciliary disk (Cd). Note that the chitin (C) is not continuous at the abfrontal tip and granulocytes (G) are migrating from the branchial sinus into the sub-epithelial space (ss and large arrow). Small arrows = myocytes.

Figure 3 Diagram showing the position and number of cells in a typical transversely sectioned *P. perna* gill filament. Ac = ciliated abfrontal cell; BS = branchial sinus; CD = ciliary disk; CLc = ciliated lateral cells; Ec = endothelial cells; Fc = frontal cells; G = granulocyte; LFc = lateral frontal cell; LMc = lateral mucus cell; Mc = mucus secreting cell; My = bridging myocyte; pc = peripheral cell; PLFc = post-lateral frontal cell; Uc = undifferentiated cell; SLc = squamous lateral cells; suffix ci = cilia.

Figure 4 Transmission electron micrograph (TEM) showing an endothelial cell (En and arrows) adhering closely to the luminal surface of chitin (C). B = branchial sinus; Ep = squamous epithelial cell.

Bivalves and methods

Mussels were collected at low tide from partly submerged rocks in the unpolluted Indian Ocean waters near Peace Cottage, Umhlanga Rocks, Natal, South Africa. Five healthy, adult mussels with shells ranging in length from 4.6 to 5.2 cm (mean 4.9 cm) were selected for evaluation. The shells were forced open and a solution of 2% glutaraldehyde in filtered fresh sea water adjusted to pH 7.2 at 22°C was poured over the gills. Undamaged areas of approximately 2 mm² were dissected through the full thickness (ascending and descending lamellae) of the central regions of each gill and placed in fresh fixative for one hour. The tissue was washed in fresh sea water, post-fixed in 1% osmium tetroxide in sea water (pH 7.2), dehydrated through graded ethanols, cleared in propylene oxide and embedded in Araldite (Glauert, Rogers & Glauert 1956) or Spurr (1969) epoxy resin.

Light microscopy and morphometry

Sections 1 µm in thickness were cut of the resin embedded tissue and stained with aqueous, alkaline toluidine blue. Areas showing cross-sectioned gill filaments were photographed and selected for electron microscopy. Measurements of gill filament width and length, cilia length and inter-lamellar and inter-filament distance were made directly from video images derived from a light microscope interfaced with a Noran 'Voyager' 2100 image analytical system. Data from at least 10 filaments were collected from each bivalve. Measurements of cytoplasmic organelles and intercellular structures were made from video images of electron micrographs.

Electron microscopy

Each block was trimmed and aligned in such a manner as to ensure that at least 10 cross-sectioned filaments were available for fine-structural evaluation. Sections of 50–80 nm were cut of cross-sectioned filaments with glass or diamond knives, picked up on uncoated copper grids and double stained with uranyl acetate and lead citrate (Reynolds 1962). Each section was examined using either a Zeiss EM10B or Philips 301 transmission electron microscope.

Results

Light microscopy

Perna perna has two gills, each composed of ascending and descending lamellae. Each lamella consisted of filaments which were 190 µm (*SD* 18 µm) in external height, 24 µm (*SD* 3.4 µm) in external width at the widest point across the abfrontal 'shoulder', 30 µm (*SD* 3.2 µm) across the midfilament 'waist' and 33 µm (*SD* 3.3 µm) across the frontal 'bulge' (Figure 1). Filaments were joined laterally along their length at regular 430 µm (*SD* 28 µm) intervals by discrete ciliary disks (Figure 2). The disk attachment zone was approximately 120 µm (*SD* 15 µm) in length. While the distance between filaments was 22 µm (*SD* 1.8 µm), the distance between adjoining abfrontal shoulders at the position of the disk was 10 µm (*SD* 0.8 µm).

Apposing filaments populating ascending and descending lamellae fitted together in a 'zipper-like' configuration — the abfrontal tips of filaments of one lamellum fitted between two filaments in the apposing lamellum. The minimum distance separating abfrontal cells on apposing filaments was 20 µm.

A branchial sinus with a maximum internal lumenal width of 21 µm passed through each filament. The lumen was partially lined by a thin sheet (0.2 µm) of endothelial cells, whose nuclei were usually situated at the abfrontal and frontal ends of each filament. A chitinous sheet supported both the endothelial and external epithelial cells. In cross-section, the chitin varied in thickness from approximately 3 µm beneath the lateral squamous epithelium to 11 µm at both the abfrontal shoulder and frontal bulge. Beneath the ciliary disk, and between the ciliated epithelial cells and the chitin sheet, was a poorly stained, perhaps fluid-filled region within which were occasional granulocytes (Figure 2). In some instances, this sub-epithelial space was up to 12 µm in width.

Of particular interest was the observation that close to, and at the position of the cilial disk, the chitin did not always fully encapsulate the branchial sinus, but formed a 'pore' through which granulocytes and other moieties within the branchial sinus could migrate from the lumen to the abfrontal and lateral sub-epithelial spaces (Figures 2 & 3). Up to four non-striated myofibres bridged the dorso- and ventro-lateral chitin sheets near the abfrontal pore. Myofibres were observed only when a filament was cross-sectioned through a ciliary disk (Figures 2 & 3).

Figure 3 describes the position and number of cells in a typical transversely sectioned *Perna perna* gill filament, as determined by light and later confirmed by electron microscopy. The following description is made from the abfrontal to frontal aspects. It is important to note that the numbers of a particular cell type and relative position of cells on a typical, transversely sectioned filament were deduced from the overall appearance of all gill filaments examined. (Slight off-centre orientation of transversely sectioned specimens was found to give a false impression of cell numbers, especially of those in the abfrontal region.)

There was a similarity in type, and in some instances numbers, of cells populating the dorso- and ventro-lateral epithelia. At the abfrontal tip of each filament were two and occasionally three off-centred ciliated abfrontal cells (**Ac**). On one side, or on rare occasions, both sides of the group of Ac were small peripheral cells (**pc**). On either side of the Ac and/or pc was a single fully differentiated mucus-secreting cell (**Mc**) and frontally, a further three or four less well differentiated, immature Mc. Next to these cells on both the dorsal and ventral surfaces was a single poorly differentiated or undifferentiated cell (**Uc**) followed by a row of eight to 11 squamous, lateral cells (**SLc**) in various stages of differentiation. In some, but not all filaments, SLc contained varying numbers of mucus droplets. When present, the amount of mucus within lateral mucous cells (LMc) increased towards the frontal region. Adjoining SLc at the abfrontal edge of the dorsal and ventral frontal bulge were a group of three or four angular, interdigitating post lateral cells (**PLc**). Five multiciliate lateral cells (**CLc**) were positioned between the PLc and a single non-ciliated, columnar postlateral frontal cell (**PLFc**). The PLFc marked the beginning of cell stratification which extended to the second or third frontal cell. Next to each PLFc was a single, large, multiciliate columnar lateral frontal cell (**LFc**), behind or to the side of which was often a single, smaller, immature LFc. The frontal aspect of each filament

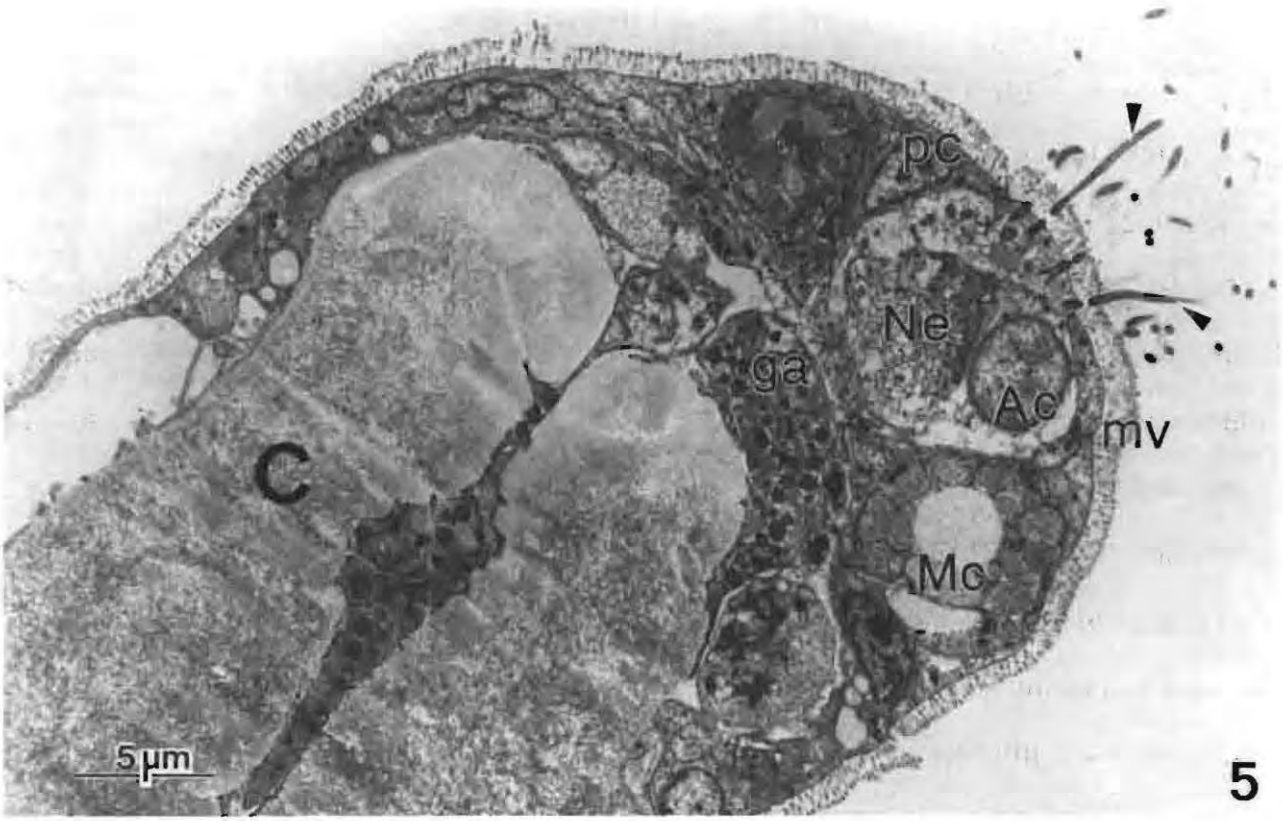

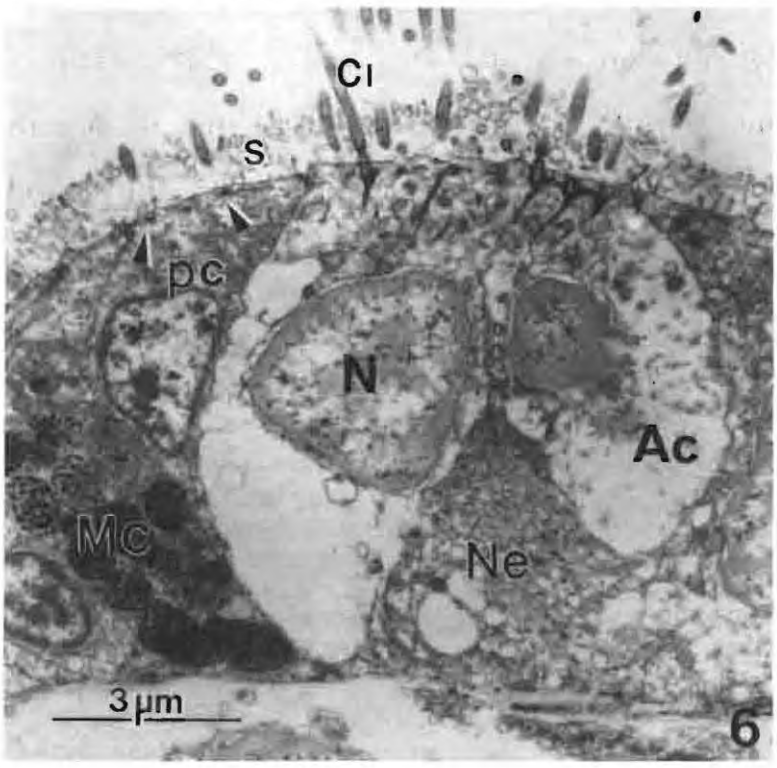

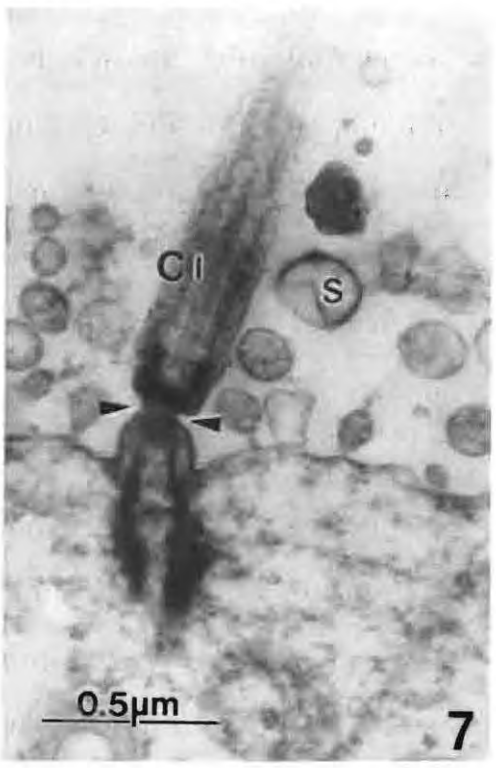

Figure 5 TEM showing the position of cells at the abfrontal region of a filament sectioned near a ciliary disk. The ciliated abfrontal cells (Ac) are almost enclosing the abfrontal nerve (Ne). Note the peripheral cell (pc) next to the Ac. Two mucus cells (Mc) are positioned on either side of the Ac complex. Note that the chitin (C) is not continuous at the abfrontal tip and type ga granulocytes (ga) occur within the sub-epithelial space. mv = microvilli; cilia — arrowed.

Figure 6 TEM. Vacuolated Ac in close proximity to the abfrontal nerve. The nucleus (N) appears necrotic — the nucleolemma is swollen and the nucleoplasm has lost most of its chromatin. Note the electron-dense ciliary rootlets (arrowed) beneath the plasmalemma of the peripheral cell. s = spherical vesicles; Ci = cilia.

Figure 7 TEM. Typical Ac cilium. Note the narrow neck (arrowed) 0.2 µm above the plasmalemma.

was populated with 10 to 12 ciliated, columnar frontal cells (Fc). Behind the first or second Fc, especially on the dorsal side of each filament, were one or two strata of smaller, perhaps immature Fc.

Electron microscopy

All epithelial cells were attached to a well-defined basement membrane by means of hemi-desmosomes. The number of cilia projecting from cell surfaces was expressed as cilia per μm^2 and determined by measurements from a minimum of five micrographs per specimen of oblique or transverse sections through cilia in the extracellular regions directly above cells.

Endothelial cells

Endothelial cells lined much of the luminal surface of the branchial sinus. These cells were up to 1 µm in height at the position of the nucleus and up to 17 µm in length (Figure 4). The cytoplasmic sheet extending over the chitin rarely exceeded 200 nm in thickness. No basal lamina and no junctional complex with the underlying chitin was seen. While endothelial cells often overlapped at their periphery, no intercellular junctions were observed.

Abfrontal cells

These cells ranged in size from 4.5 to 5 µm in width and 6.5 to 8.8 µm in height (Figures 5 & 6). Each cell contained a single, electron-pale, rounded nucleus approximately 3.6 µm in diameter within which was a flocular nucleosol. Mitochondria were sparse and small, the nucleolemma was generally swollen and the cytosol was vacuolated and rarely contained any other distinctive organelles. Projecting from the surface were rows of cilia approximately 0.16 µm apart and with a density of 8 cilia/μm^2. Each cilium was 0.26 µm in diameter, up to 6 µm in length and contained the conventional nine outer and single inner pairs of microtubules. Approximately 0.2 µm above the cell surface was a thin (600 nm) 'neck' to each cilium (Figure 7). The nine outer paired microtubules of each cilium appeared to fuse into an electron dense region just above the neck while the central paired microtubules passed through the neck to be anchored into the cytosol by short (0.9 µm), sometimes paired rootlets. The cilia were interspersed by microvilli that in most instances appeared to have degenerated into membrane-bound vesicles. Occasional necrotic abfrontal cells were exfoliating into the extra-cellular space.

Adjoining one or both Ac was a small 'peripheral' cell (Figures 5, 6 & 8). These cells ranged from 3 to 4.5 µm in width and appeared to extend to the basal lamina. The cytoplasm contained strands of rough endoplasmic reticulum (RER), occasional small mitochondria and numerous ribosomes. The single irregularly shaped nucleus contained large amounts of peripheral chromatin. While no cilia were seen projecting from these cells, the presence of sub-plasmalemal osmiophilic rootlets suggested that the cells may be ciliated (Figure 6).

Mucus cells

Up to four mucus secreting cells occupied positions on the abfrontal shoulder. In rare instances, all four cells were packed with mucus droplets (Figure 8), in others, very few mucus droplets were present in any cell (Figure 9). The most common arrangement was a single, well developed Mc on either side of the pair of Ac followed by three less well differentiated cells (Figure 5). Each actively secreting Mc was approximately 5 µm in width and 7.5 µm in height and contained numerous mucus droplets. There was usually a progressive positional decrease in the height and width of Mc, size of their nuclei and numbers and size of secretory granules with distance from Ac. The less well differentiated Mc exhibited much RNA activity, had well developed Golgi apparatus and contained numerous strands of rough endoplasmic reticulum (RER). Irrespective of their stage of differentiation, numerous microvilli, 0.4 to 0.5 µm in length, projected from the Mc surface and were connected laterally by an electron-dense glycocalyx.

Undifferentiated cells

Adjoining poorly differentiated Mc was a single undifferentiated cell (Figure 9). These small cells rarely exceeded 3 µm in width and 6 µm in height, had an irregular shaped nucleus and a cytosol within which were occasional small mitochondria, ribosomes and strands of RER. Numerous microvilli projected up to 0.5 µm from the luminal surface of each cell.

Squamous lateral cells

From the undifferentiated cell/lateral cell interface to the centro-lateral position, there was a gradual transformation in cell shape from cuboidal to squamous. Next to undifferentiated cells, SLc were from 3 to 4 µm in width and up to 6 µm in height. Other than that most cells did not contain secretory droplets, these cells were morphologically similar to the poorly differentiated cells described above. Centro-lateral cells were from 1 to 1.3 µm in thickness, up to 14 µm in length and contained elongated nuclei, a few small electron-dense mitochondria and occasional strands of RER and aggregates of glycogen (Figures 10 & 11). There were some rare instances of 1 or 2 cilia projecting from centro-lateral cells (Figure 11). From the centro-lateral region to the interface with post-lateral cells, SLc became more cuboidal. The cytosol of these cells was sometimes vacuolated and contained degenerate mitochondria and swollen smooth ER. Occasional exfoliating cells were observed in this position.

The lateral cells populating some filaments contained mucus droplets. When present, there was a progressive increase in the number of mucus droplets in cells positioned nearer to the frontal regions. Close to the SLc/PLc interface, lateral mucus cells (LMc) appeared fully differentiated with some exocytosing their mucus into the interfilamentar space (Figure 12). Irrespective of position or mucus content, projecting from the surface of all SLc were numerous short microvilli (0.4–0.5 µm), connected laterally by an osmiophilic glycocalyx.

Postlateral cells

These three or four triangular-shaped cells were connected laterally by interdigitating processes. In some instances, the cells were only loosely connected to each other and the basement membrane by elongated pseudopodia. Each cell contained a round/oval nucleus within which was often a

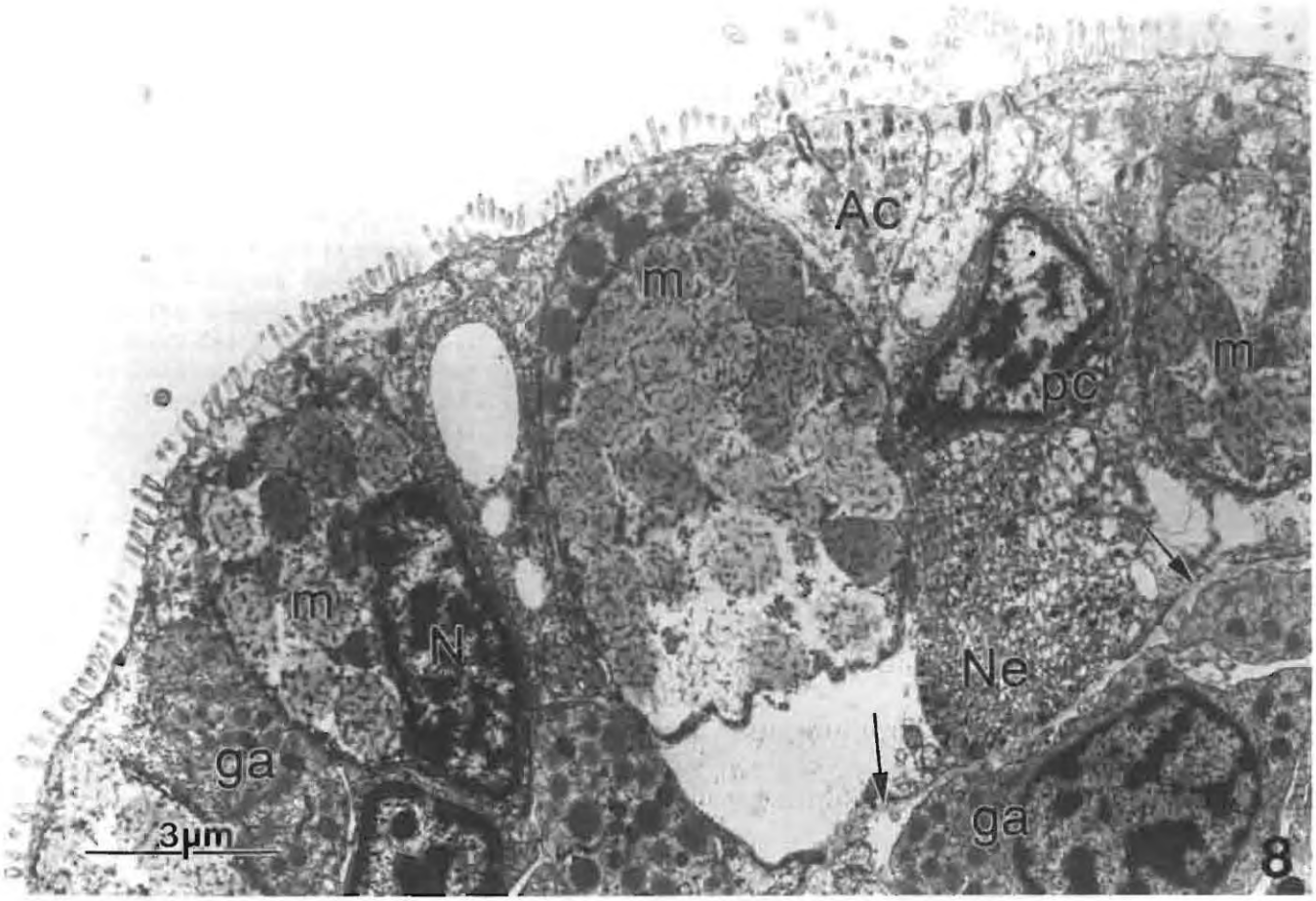

Figure 8 TEM. Mucous cells (Mc) on the abfrontal shoulder. Note the large quantities of mucus (m) within Mc. Granulocytes (ga) are present in the sub- and inter-epithelial cell spaces. Basement membrane indicated by arrows.

Figure 9 TEM. Group of poorly differentiated mucus cells (pMc). Note the undifferentiated cell (Uc) at the base of the abfrontal shoulder.

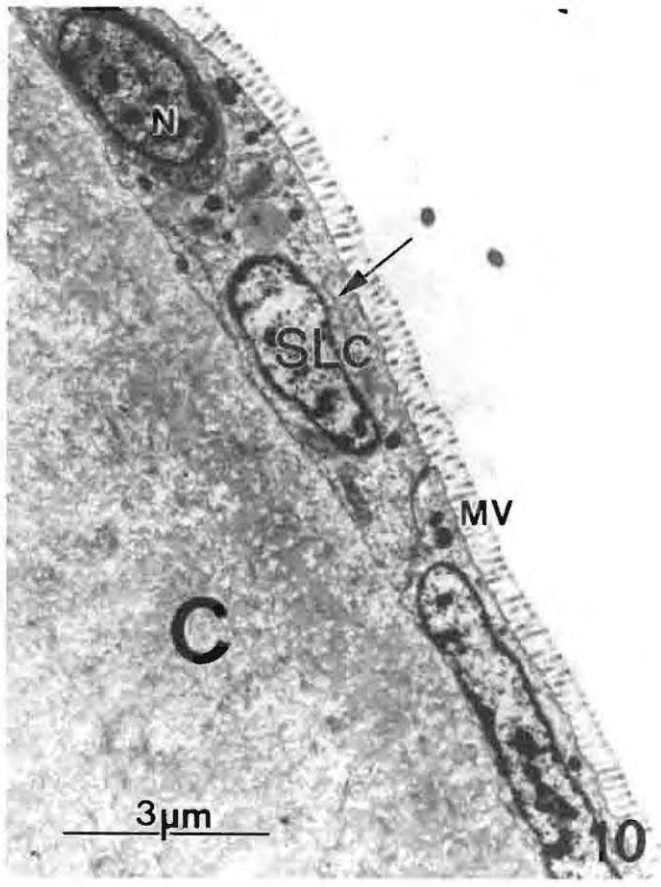

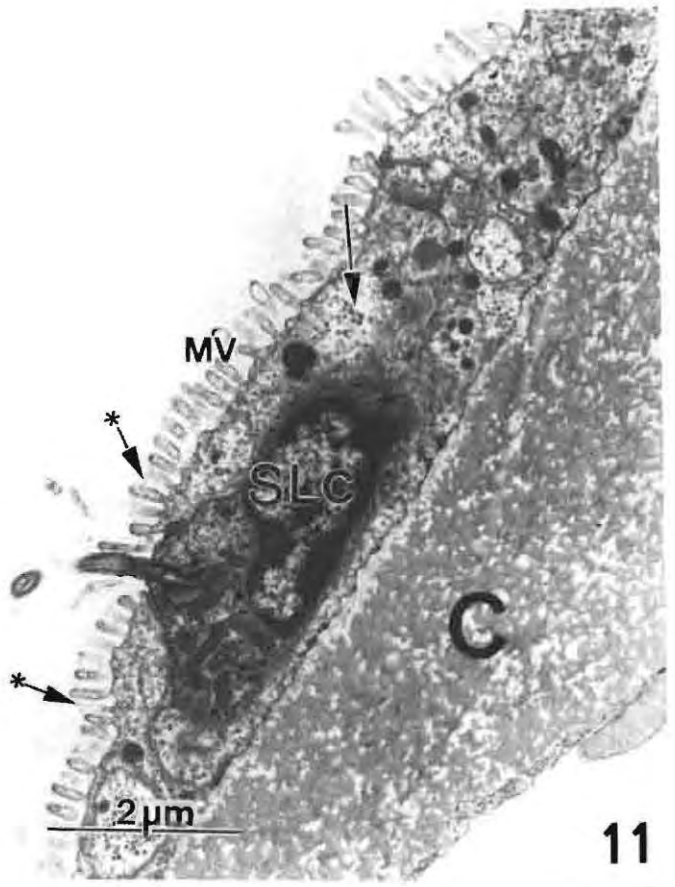

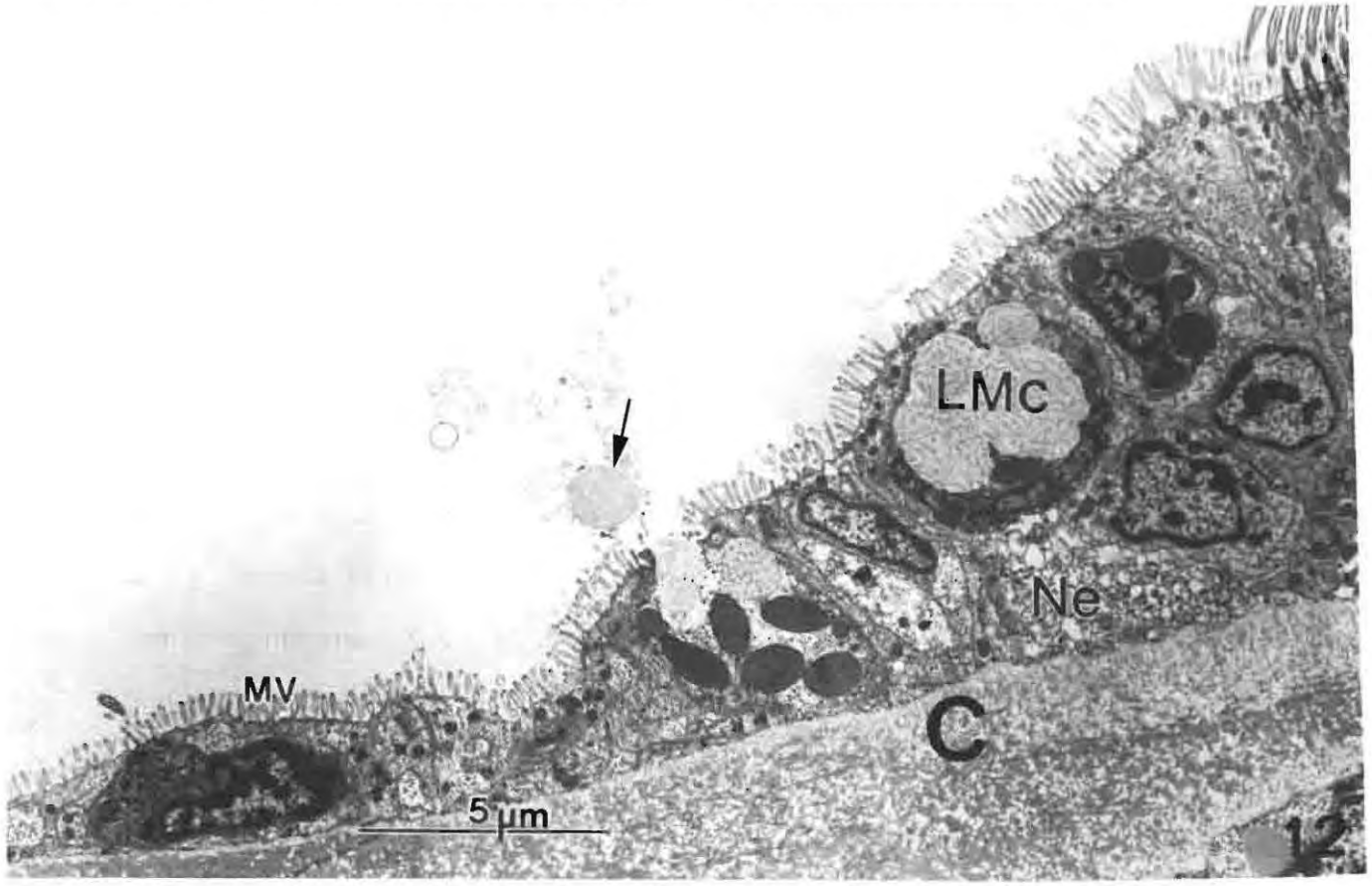

Figure 10 TEM. Centro-lateral squamous cells (SLc). Note numerous microvilli (MV) projecting from the cell surface. RER indicated by arrow.

Figure 11 TEM. Ciliated lateral squamous cell with a single cilium projecting from the cell surface. Note glycocalyx between MV (*arrows) and glycogen (arrow).

Figure 12 TEM. Actively secreting (arrow) lateral mucous cells (LMc). Ne = post-lateral nerve 1.

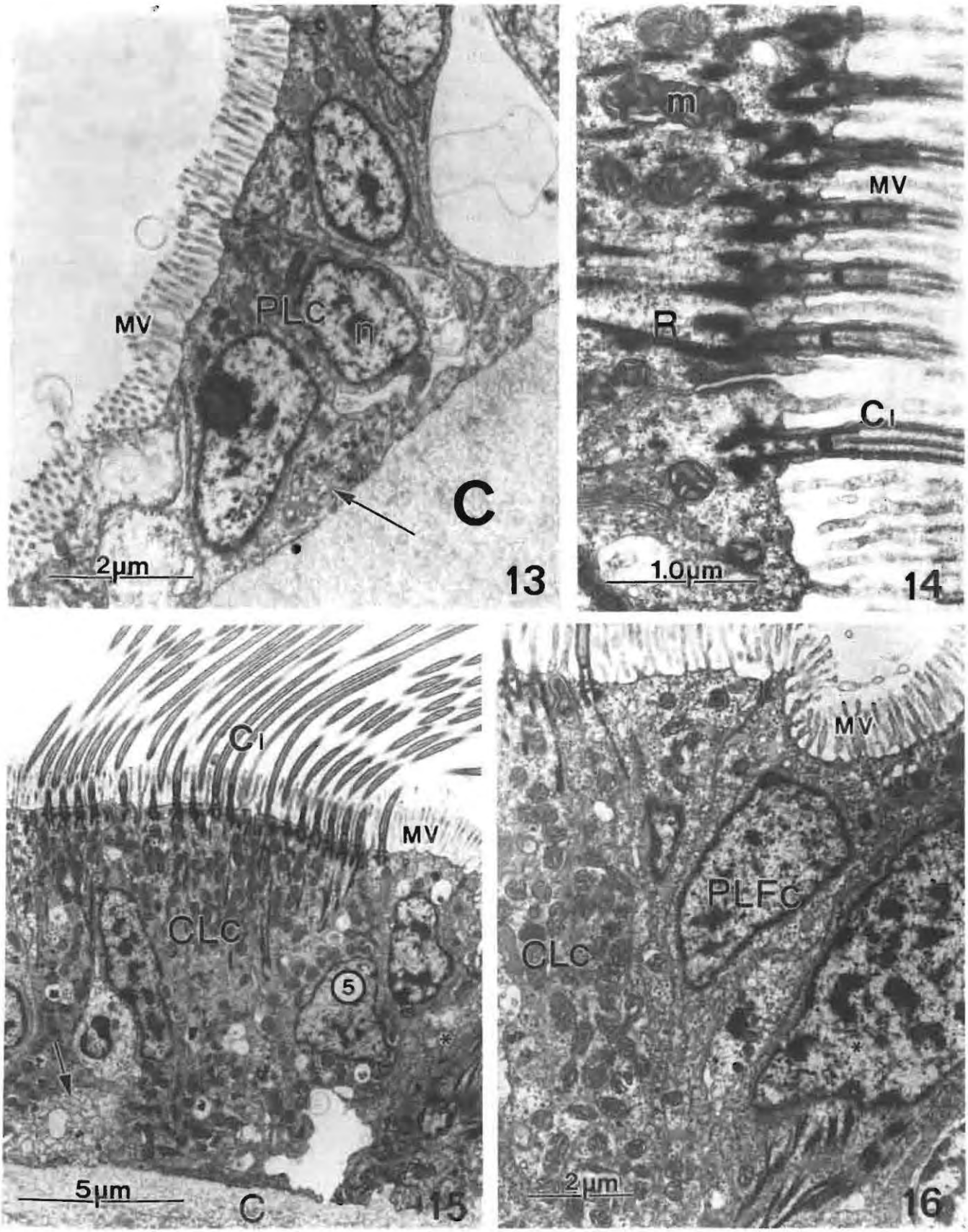

Figure 13 TEM. A typical group of three post-lateral cells (PLc). Note increased length of MV when compared with those projecting from squamous cells (Figures 10–12). Post-lateral nerve 1 shown by arrow.

Figure 14 TEM. Detail of cilia projecting from ciliated lateral cells. The cilia are anchored within the cytoplasm by rootlets (R). Note the long, single microvillous between each cilium. m = mitochondria.

Figure 15 TEM. Five multi-ciliate lateral cells (CLc). The fifth cell (5) has only a single cilium projecting from its surface. Note necrotic regions within the cytoplasm of the post-lateral frontal cell (*). Post-lateral nerve 2 shown by arrow.

Figure 16 TEM of healthy post-lateral frontal cell (PLFc) between fifth CLc and ciliated lateral frontal cell (*).

prominent nucleolus (Figure 13). The cytoplasm contained occasional strands of RER, ribosomes, occasional Golgi cisternae and large mitochondria within which were numerous cristae. Numerous microvilli, up to 0.8 µm in length, projected from the cell surface.

Multi-ciliate lateral cells

These five ciliated columnar cells were up to 3.5 µm wide, up to 15 µm long and characterized by numerous quite large mitochondria randomly distributed between well-defined cilia rootlets (Figure 14). Cilia, arranged in rows approximately 0.3 µm apart, were 0.25 µm in diameter, up to 21 µm in length and regularly interspersed by microvilli (Figure 15). There were 9 cilia/µm^2 projecting from the entire surface of each of the first four CLc. The fifth CLc, in cross-section, was characterized by having either a single cilium or reduced numbers of cilia (Figures 15 & 16).

Post-lateral frontal cell

This single non-ciliated columnar cell was from 2.5 to 3.5 µm in width and up to 15 µm in height. These cells varied dramatically in appearance. Some cells contained numerous ribosomes, long strands of RER, occasional small mitochondria and a nucleus with large quantities of centrally located and peripheral chromatin (Figure 16), while in others the cytoplasm was electron-lucent, generally vacuolated and lacking intact organelles (Figure 15). Although non-ciliated, PLFc often contained the remnants of cilia rootlets within the subplasmalemmal cytosol. Necrotic PLFc were sometimes observed exfoliating from the filament epithelium.

Lateral frontal cell

These large, ciliated columnar cells were from 9 to 10 µm in width and up to 19 µm in height (Figure 17). They contained an elongated nucleus in a moderately electron-lucent cytosol. Small, sparse mitochondria were particularly aggregated about the cilia rootlets and a well-developed Golgi apparatus was present in many cells. Multiple paired rows of cilia, approximately 0.25 µm in diameter, projected up to 18 µm into the extra-cellular space. Each paired row was approximately 2.3 µm from the other and in a pair the rows were 0.13 µm apart. A particularly electron-dense terminal web appeared to connect the cilia just beneath the plasmalemma. Numerous microvilli with a density of approximately 50Mv/µm^2 interspersed the cilia and projected up to 1.6 µm from the cell surface. There was often a smaller cell either lateral to or behind mature LFc. These cells had similar cytoplasmic and nuclear characteristics to LFc and appeared to be immature cells.

Frontal cells

The columnar frontal cells adjoining the ventral and dorsal LFc on the surface of each filament were up to 15 µm long, approximately 2.5 µm wide and contained a single, elongated, thin nucleus (Figure 18). The cytosol contained occasional strands of RER, a well-developed Golgi apparatus and moderately electron-dense mitochondria with well-defined cristae. Behind these Fc, especially on the dorsal side, were one or two strata of cells with the characteristic appearance of poorly differentiated cells (see above). Towards the middle of the frontal region, frontal cells became increasingly more cuboidal with widths up to 6 µm and height from 8 to 10 µm. Many contained numerous autophagic vacuoles. In such cells, nuclei became increasingly rounded and pyknotic, the cytoplasm gradually lost its electron density and appeared empty and there was a reduction in the amount of both RER and smooth ER (Figure 19). The Golgi apparatus was less evident and mitochondria were often swollen. Necrotic cells were observed exfoliating from this position.

All frontal cells had two parallel, juxtaposed rows of cilia 0.16 µm apart. The paired cilia were, on average, 8.9 µm in length and 0.25 µm in diameter. The cilia were anchored within the cell by a pair of rootlets that penetrated into the cytosol (Figure 20). The entire cell surface was covered with numerous, sometimes branched microvilli with a density of approximately 30 Mv/µm^2. Each microvillus was 0.08 µm in diameter and projected up to 1.2 µm into the extracellular space. There appeared to be a single row of microvilli between the paired rows of cilia. Approximately 0.7 µm from the cell surface, microvilli were joined laterally by a moderately electron-dense glycocalyx.

Ciliary discs

Each disc comprised a group of nine multiciliate cells that were situated in positions otherwise occupied by lateral cells (Figure 21). The first cell adjoining the poorly differentiated cell on the abfrontal shoulder had few cilia and contained a well-developed Golgi apparatus and abundance of glycogen and ribosomes. Seven multi-ciliate cells comprised the main body of the ciliary disk. These were from 6 to 6.6 µm wide at their ciliated surface and from 7.2 to 11.2 µm in height. The cells were attached to the basement membrane by invaginating foot processes and hemi-desmosomes. Nuclei appeared as elongated ovals approximately 2 µm in diameter and up to 7.5 µm in length. The cytoplasm contained occasional multivesicular bodies and numerous vesicles, from 0.18 to 0.3 µm in diameter, within which was a moderately electron-dense, amorphous material. The vesicles appeared to be more numerous in the cells closer to the frontal regions. The cell at the frontal position of each disk had few cilia and was characterized by the presence of cytoplasmic vacuoles and swollen mitochondria.

The cilia were 2.5 µm in diameter and appeared similar to those projecting from CLc. A notable difference was the length of cilia rootlets which in cilial cells penetrated through the cytoplasm to the basal plasmalemma. The interdigitation of cilia from cells in lateral filaments made it difficult to determine ciliary length. However, the distance between filaments bridged by cilia was approximately 12 µm at the narrowest point. The disk was composed of 9 cilia/µm^2.

Myocytes

These were only observed when a filament was cut through a ciliary disk. A maximum of four individual myocytes was seen bridging the dorsal and ventral chitinous sheets beneath ciliary disks (Figure 22). Each cell bridged a gap of approximately 9.5 µm and was separated from its neighbour by a distance not exceeding 2.8 µm. The cells were approximately 9.5 µm in length and 4 µm in diameter. They contained a single,

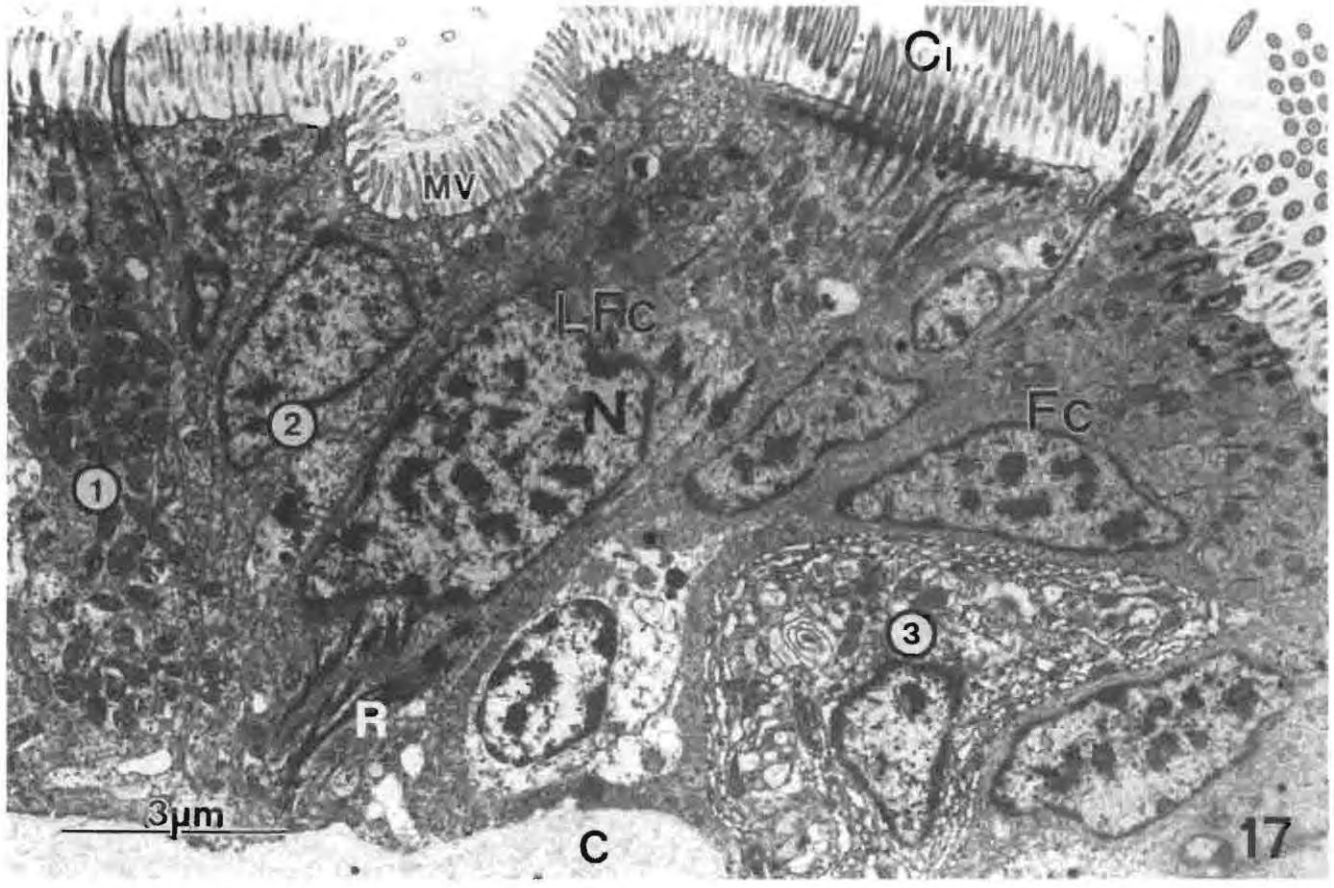

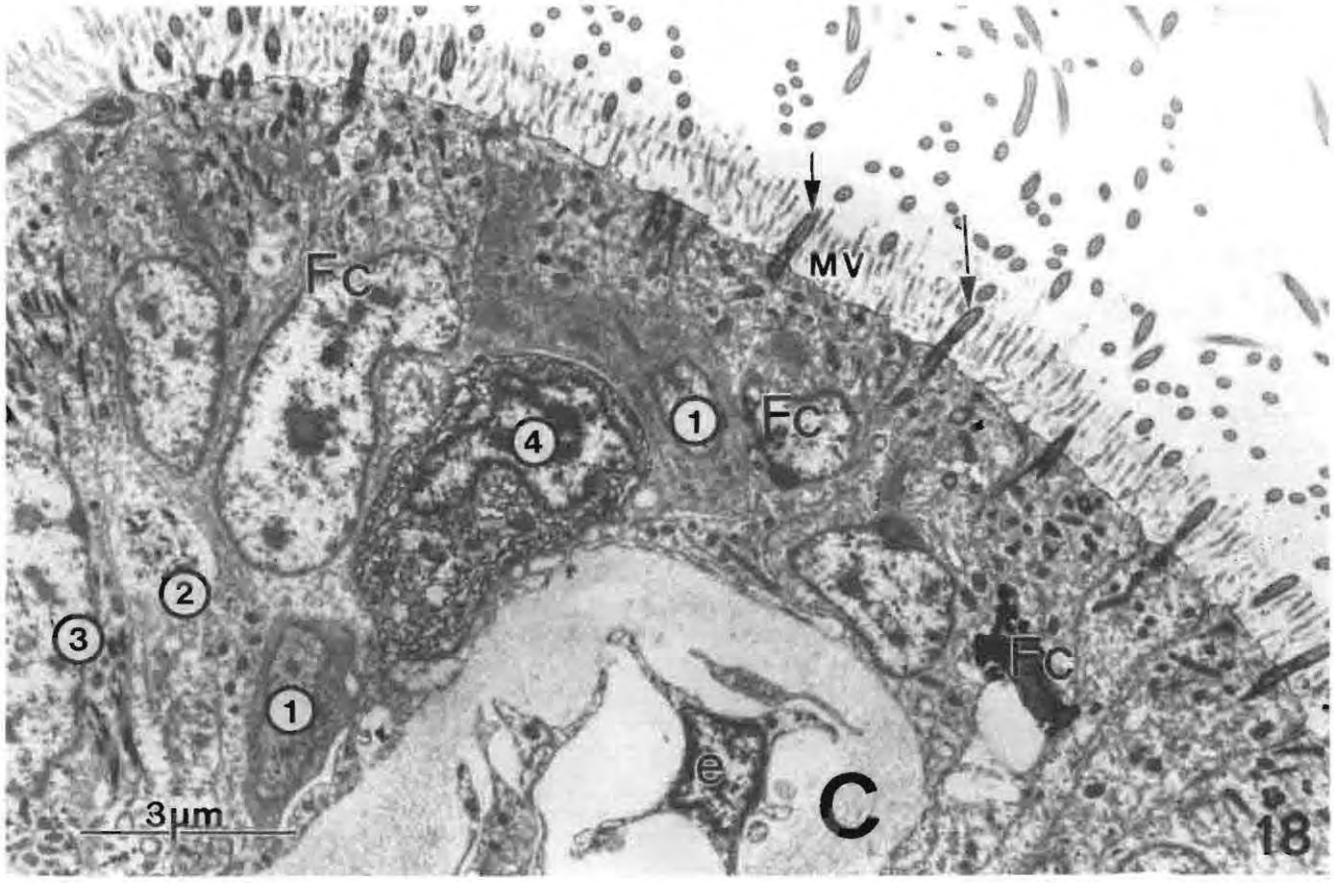

Figure 17 TEM of frontal bulge showing position of a ciliated lateral frontal cell (LFc) and apparent stratification of cells at the lateral frontal and frontal cell interface. Note the cilia rootlets (R) stretching through the full length of the LFc. Fc = frontal cell; 1 = CLc; 2 = PLFc; 3 = necrotic frontal cell.

Figure 18 TEM of frontal region showing ciliated frontal cells (Fc). Note the poorly differentiated, perhaps germinal cells (1) within the lower strata of cells at the lateral frontal and frontal cell interface. 2 = necrotic LFc; 3 = LFc; 4 = necrotic Fc; cilia (arrowed); e = endothelial cells.

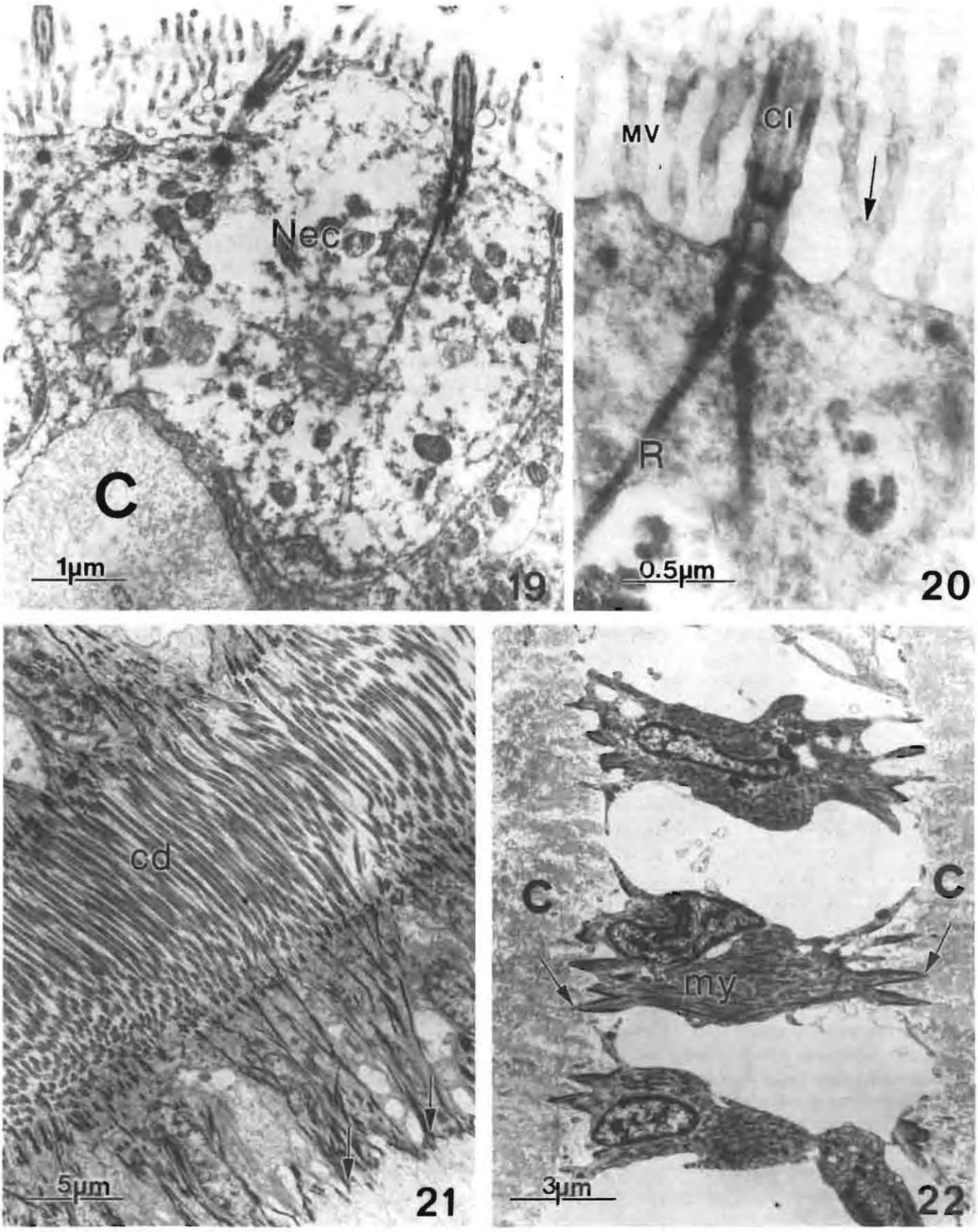

Figure 19 TEM. Necrotic (Nec), exfoliating Fc.

Figure 20 TEM. Detail of Fc cilium and paired rootlets. Note the elongated, branched MV (arrowed) projecting from the cell surface.

Figure 21 TEM. Interdigitating cilia comprising the ciliary disk (cd). Note that the rootlets stretch through the cell and anchor on the basal plasmalemma (arrowed).

Figure 22 TEM. Myocytes (my) bridging the dorsal and ventral chitin sheets at the position of the ciliary disk. Note that myocyte attachments appear to penetrate into the chitin (arrows).

elongated nucleus up to 1.3 µm in diameter and 4.7 µm in length. The sarcosol was filled with strands of electron-dense myosin, more electron-pale actin and very occasional, small mitochondria. The myocytes were attached to the chitinous sheet on both sides by processes which penetrated into the chitin. The processes did not appear to attach to a basement membrane but to the chitinous filaments of the sheet via electron-dense hemi-desmosomes.

Epithelial cell junctions

Irrespective of their position on the filament, epithelial cells were joined by a common septate junction complex. Each complex consisted of an outer zonula adherens (loose junction) and an inner septate junction (Figure 23). The zonular adherens was typically up to 22 µm in length and the gap between cells approximately 29 nm. At the base of the loose junction, the gap between cells narrowed to 17 nm. At this point, the lateral plasmalemmae were joined by numerous horizontal septa 8 nm in thickness and 10 nm apart (Figure 24). Septate junctions ranged in length from 87 nm (6 septa) to 200 nm (13 septa).

Amoeboid cells

Amoeboid cells were generally contained within the lumen of the branchial sinus. They did, however, appear to gain passage to the surface epithelium through the abfrontal gap in the chitinous sheet at the position of the ciliary disk. From this position, they migrated to all parts of the filament. Two primary types of amoeboid cells were identified: non-granulocytes and granulocytes.

Granulocytes were of two types: **ga**, large cells with amorphous granules (Figure 25); and **gb**, smaller cells whose granules contained osmiophilic bars (Figure 26). Both types were found in the branchial sinus and in the intercellular spaces between epithelial cells. Within the branchial sinus, the largest ga recorded was 5.5 µm in diameter and 7.7 µm in length. However, in the interstitial spaces, the cells could elongate to lengths in excess of 10 µm. The nucleus was generally rounded, approximately 2.8 µm in diameter and contained large quantities of peripheral and centralized chromatin. The cytoplasm contained numerous membrane-bound granules of varying electron densities that ranged from 0.3 to 0.6 µm in diameter.

The smaller gb were often observed in the intercellular spaces, especially near the post-lateral nerves (Figure 26). The cells were rarely larger than 8 µm in diameter and contained dense membrane-bound, oval granules up to 0.8 µm long. Each granule was characterized by the presence of an elongated electron-dense rod within the granule matrix. The cytoplasm was extremely rich in ribosomes, RER and smooth ER and contained small, round/oval mitochondria with well-defined cristae. The nuclei were generally small and round and contained large amounts of peripheral chromatin.

The smaller amoeboid non-granulocytes were often present within the branchial sinus and occasionally in the intercellular spaces between epithelial cells (Figure 25). These cells were approximately 4 µm in diameter with a large rounded nucleus. The cytosol contained a few small mitochondria, strands of RER and occasional small osmiophilic granules.

Innervation

The intraepithelial position of peripheral nerves in transversely sectioned gill filaments is shown in Figure 27. All nerves were cross-sectioned suggesting that neural pathways extended along the length of each filament. Each nerve was not myelinated and consisted of numerous irregularly shaped cross-sectioned axons ranging from approximately 0.16 to 0.33 µm in diamter. Each axon contained occasional particles of glycogen and tiny cross-sectioned mitochondria from 0.1 to 0.2 µm in diameter. There were a few electron-dense vesicles in each nerve that may represent neural tubules.

Six nerves were detected: Abfrontal (1); post-lateral-1 (2); post-lateral-2 (2); and lateral-frontal (1). The abfrontal nerve was the largest in cross-section being up to 4 µm in diameter (Figures 5, 6 & 8). It was situated directly beneath, and enveloped by, the basal regions of the ciliated abfrontal cells. The bi-lateral, post-lateral-1 nerves were approximately 1.2 µm in diameter and situated beneath the first or second post-lateral cells (Figures 13, 25 & 26). The bi-lateral, post-lateral-2 nerves were the smallest, being from 0.9 to 1.8 µm in diameter. They were situated directly beneath the first ciliated lateral cell on each surface (Figure 15). The lateral-frontal nerve was approximately 1.1 µm in diameter and situated beneath and between the latero-frontal and first frontal cell. This nerve was only found on the dorsal surface.

Discussion

Gills are key organs in bivalves, while bivalves are often, in turn, key species in marine ecosystems. The functional anatomy of bivalve gills is thus of broad fundamental interest to marine biologists and has received wide attention. While many of the early studies were comprehensive in terms of coverage, they were technically limited by the absence of photomicrography, electron microscopy and modern histological techniques (Ridgewood 1903; Rice 1908; Atkins 1936, 1937a,b,c, 1938a,b,c, 1943). Latterly, a number of workers have applied the new techniques to enhance our understanding of the microstructure and function of bivalve gills. A detailed literature review will not be attempted here, instead, a few articles will be cited to provide an idea and the scope of the more recent work.

Owen (1978) used scanning and transmission electron microscopy to elucidate the fine-structure of bivalve gills and so gain insight into phylogenic relationships. LePennec, Beninger & Herry (1988) and Beninger, LePennec & Salaun (1988) focussed their attention on the anatomy of gills from the scallop *Placopecten magellanicus* and were able to draw some conclusions regarding nutrition mechanisms. Sunila (1986) provided a detailed account of the histology and general organisation of gill filaments in the blue mussel *Mytilus edulis* to provide a baseline for his later work on the effects of pollution on gill structure (Sunila 1987, 1988). *Mytilus edulis* was also the focus of studies by Hietenan *et al.* (1988) and Ballan-Dufrancais, Jeantet & Coulon (1990) who investigated the histopathological effects of zinc and titanium dioxide effluent, respectively, on gill tissue. Good, Stommel & Stephens (1990) and Stephens & Good (1990) further refined our understanding of gill ultrastructure in *Mytilus edulis* and *Aequipecten irradians*, while Jones, Richards & Hutchinson (1990) gained additional insight into the hydrodynamics of

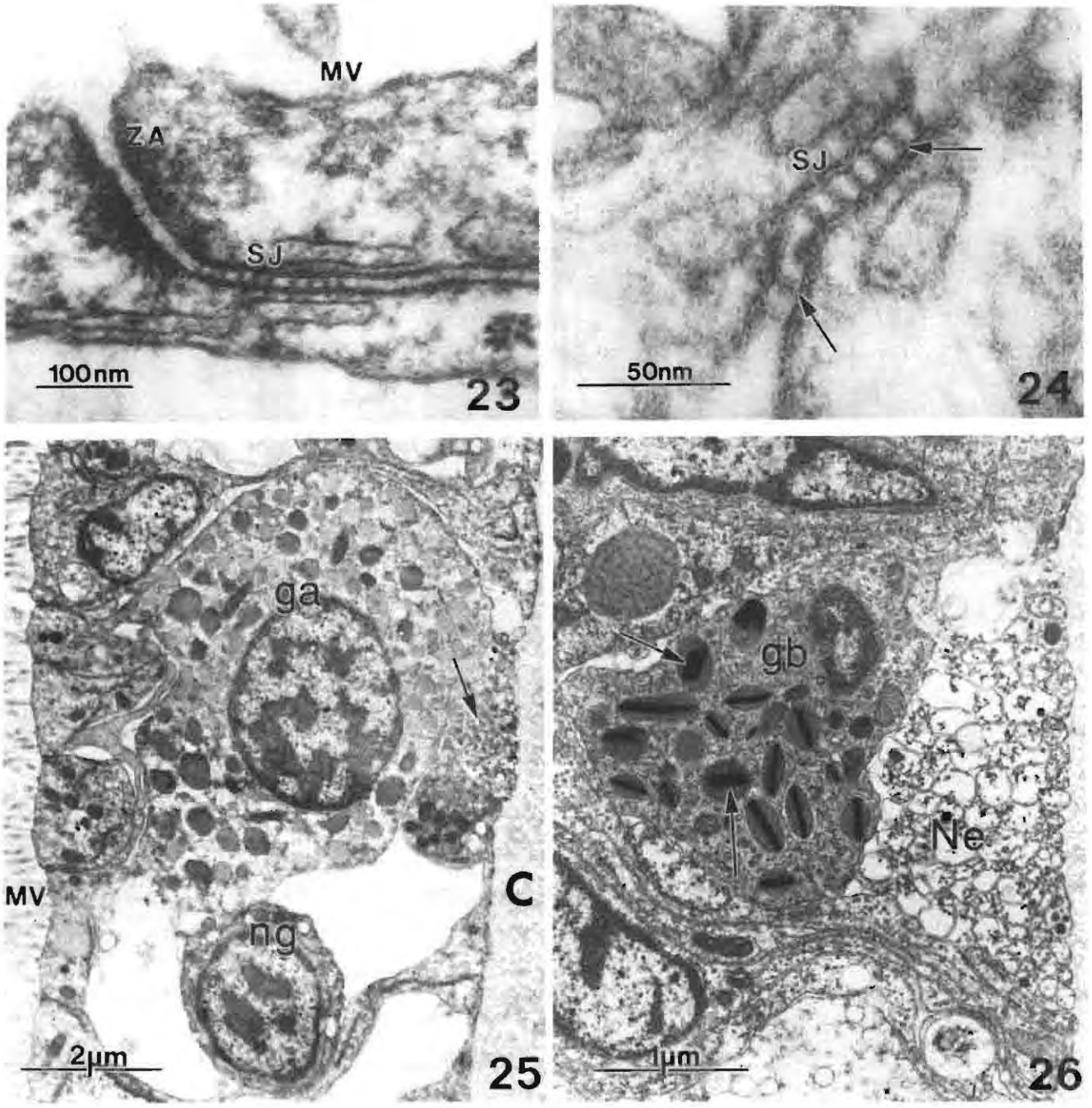

Figure 23 TEM of SLc septate junction. ZA = zonular adherens; SJ = septate junction.
Figure 24 TEM of PLc septate junction. Note the clearly defined septa within the septate junction.
Figure 25 TEM of amoeboid cells in the post-lateral intercellular space. Note the amorphous, generally spherical granules within type ga granulocytes. ng = typical non-granulocyte; post-lateral-1 nerve shown by arrow.
Figure 26 TEM of type gb granulocyte in the post-lateral intercellular space. Note the electron-dense bars within oval granules (arrowed). Ne = post-lateral-2 nerve.

water pumping in *Mytilus edulis* through their micro-anatomical observations. It is evident from the available literature that *Mytilus edulis* has received considerable attention. Nothing comparable has hitherto been published on *Perna perna*. A number of differences exist between the two species.

In *Mytilus edulis*, the integrity of the gill filament is reportedly maintained by single rows of smooth muscle fibres at both the frontal and abfrontal regions of the branchial sinus (Sunila 1986). In *Perna perna*, up to four smooth myocytes bridged the thickened abfrontal, dorsal and ventral walls of the vessel, but only where filaments were connected by ciliary disks. No myocytes bridged the thickened frontal dorsal and ventral walls, instead the narrow space between the chitinous sheets was bridged by processes from endothelial cells.

These substantial positional and numeric differences in myocytes may be due to generic or specific variations in the distribution and thickness of chitin. In addition to serving as a rigid support for endothelial and epithelial cells, chitin helps to maintain the shape of each gill filament. In *Mytilus edulis*, the chitin underlying lateral frontal cells is quite thin (Sunila, 1986) whereas in *Perna perna*, the dorsal and ventral lateral-frontal chitin sheets were particularly thickened. These archi-

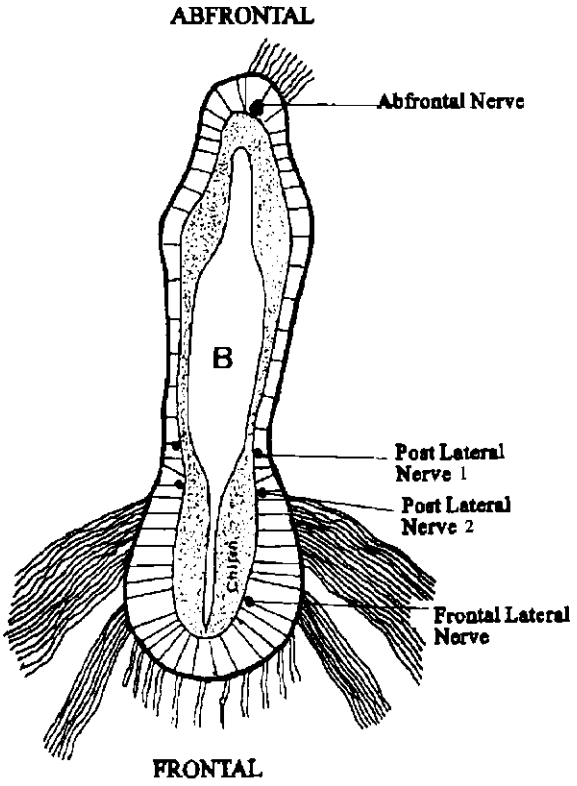

Figure 27 Diagram showing the innervation of a transversely sectioned filament.

tectural differences lead us to postulate that a bridging myocyte is necessary to maintain the frontal shape of the filament in *Mytilus edulis*, whereas in *Perna perna*, frontal shape is adequately maintained by thickened chitin.

Change in the shape of gill filaments is recognized as a primary response of *Mytilus edulis* to toxic metal pollution and has been ascribed to a slacking of the frontal and abfrontal muscles and consequent dilation of the branchial vein (Sunila 1986). The presence of thicker chitinous support, and up to four bracing myocytes, in *Perna perna*, suggests that this species has stronger and more resilient gill filaments which would be less likely to become distorted under stress.

Mytilus edulis and *Perna perna* gill filaments differ markedly in the location and mechanism of mucus secretion. In *Mytilus edulis*, mucus is reportedly synthesized by, and secreted from, small glands situated beneath the ciliated abfrontal cells (Sunila 1986). In *Perna perna*, mucus appears to be progressively synthesized within immature secretory cells as they migrate abfrontally, with mucus being secreted from one or more fully differentiated cells situated on either side of the peripheral cells or group of abfrontal cells. Further, on some filaments it appears that mucus is also synthesized within some cells as they migrate frontally. In such circumstances, mucus is secreted from mature cells situated at or near the lateral cell/post-lateral cell junction. This mechanism of progressive differentiation and muco-synthesis eventuating in merocrine muco-secretion from mature mucous cells is similar to that adopted by goblet cells in the secretory epithelia of the mammalian small intestine (Gregory & Spitaels 1987).

There were also considerable differences in the numbers and position of particular types of epithelial cells lining the filaments of both species of mussel. In *Mytilus edulis* there were four off-centred, ciliated abfrontal cells whereas in *Perna perna*, there were never more than three ciliated cells in this position — one being possibly a nearly mature peripheral cell. *Mytilus edulis* had only two post-lateral cells while *Perna perna* had three or four. In *Mytilus edulis*, only four frontal cells were described whereas in *Perna perna* up to 11 cells were observed. In *Mytilus edulis*, the epithelium was a simple mono-layer over the entire filament whereas the cells populating the frontal bulge of *Perna perna* were stratified.

While there were considerable species differences in the architecture of filament epithelia, the cilia projecting from particular cell types in *Perna perna* were similar to those described in *Mytilus edulis*. The cilia could be loosely divided into two morphological types: 'necked' and 'no-necked'. Necked cilia were only found projecting from abfrontal cells and were characterized by a narrowing of the shaft of the cilium just above the cell surface and short, sometimes paired rootlets within the cytosol. Cilia projecting from lateral, lateral-frontal, frontal cells and those comprising the cilial disk were uniform in diameter along their length and were anchored within the cytosol by long rootlets which in the case of ciliary cells extended to the basal plasmalemma. These current-producing, particle-carrying and filament-bridging cilia appeared far more robust than the more architecturally fragile, tactile cilia projecting from the abfrontal sensory cells.

This article has described the morphology and architecture of gill filaments in *Perna perna* and has drawn some comparisons with *Mytilus edulis*. It is hoped that this comprehensive description will provide a basis for local studies on the response of *Perna perna* to pollution.

Acknowledgements

The authors would like to thank the CSIR and the Foundation for Research Development (FRD) for their continuing support for this project. Also our thanks to Mrs A. Naicker and Mrs S. Bux of the Department of Physiology, Medical School, University of Natal for their technical assistance during the early stages of the study.

References

ANDERLINI, V.C. 1990. The effect of sewage on trace metal concentrations and scope for growth in *Mytilus edulis aoteanus* and *Perna canaliculus* from Wellington Harbour, New Zealand. Paper presented at the International Conference on Trace Metals in the Environment, Sydney (Australia), July 1990. In: Trace metals in the aquatic environment, (ed.) G.E. Batley. 125: 263–288 (1992).

ANON. 1980. The International Mussel Watch. Report on a workshop sponsored by the Environmental Studies Board, Commission on Natural Resources and National Research Council. National Academy of Sciences, Washington D.C. pp. 248.

ATKINS, D. 1936. On the ciliary mechanisms and interrelationships of lamellibranchs. Part I: New observations on sorting mechanisms. *Q. J. microsc. Sci.* 79: 181–308.

ATKINS, D. 1937a. On the ciliary mechanisms and interrelationships of lamellibranchs. Part II: Sorting devices on the gills. *Q. J. microsc. Sci.* 79: 339–373.

ATKINS, D. 1937b. On the ciliary mechanisms and interrelationships of lamellibranchs. Part III: Types of lamellibranch gills and their food currents. *Q. J. microsc. Sci.* 79: 375–421.

ATKINS, D. 1937c. On the ciliary mechanisms and interrelationships of lamellibranchs. Part IV: Cuticular fusion. *Q. J. microsc. Sci.* 79: 423–445.

ATKINS, D. 1938a. On the ciliary mechanisms and interrelationships of lamellibranchs. Part V: Notes on the gills of *Amussium pleuronectes* L. *Q. J. microsc. Sci.* 80: 321–329.

ATKINS, D. 1938b. On the ciliary mechanisms and interrelationships of lamellibranchs. Part VI: Pattern of the lateral ciliated cells of gill filaments. *Q. J. microsc. Sci.* 80: 331–344.

ATKINS, D. 1938c. On the ciliary mechanisms and interrelationships of lamellibranchs. Part VII: Latero-frontal cilia of the gill filaments and their phylogenic value. *Q. J. microsc. Sci.* 80: 345–436.

ATKINS, D. 1943. On the ciliary mechanisms and interrelationships of lamellibranchs. Part VIII: Notes on gill musculature in the microciliobranchia. *Q. J. microsc. Sci.* 84: 187–256.

BALLAN-DUFRANCAIS, C., JEANTET, A.Y. & COULON, J. 1990. Cytological features of mussels (*Mytilus edulis*) in situ exposed to an effluent of the titanium dioxide industry. *Ann. Inst. Oceanogr.* Paris, 66: 1–18.

BENINGER, P.C., LePENNEC, M. & SALAUN, M. 1988. New observations of the gills of *Placopecten magellanicus* (Mollusca: Bivalvia) and implications for nutrition. I: General anatomy and surface micro-anatomy. *Mar. Biol.* 98: 61–70.

BOCQUENE, G., GALGANI, F., BURGEOT, T., LE DEAN, L. & TRUQUET, P. 1993. Acetylcholinesterase levels in marine organisms along the French coast. *Marine Pollution Bulletin* 26: 101–106.

COLES, J.A., FARLEY, S.R. & PIPE, R.K. 1994. Effects of fluoranthene on the immunocompetence of the common mussel, *Mytilus edulis*. *Aquatic Toxicology* 30: 367–379.

GARDNER, B.D., CONNELL, A.D., EAGLE, G.A., MOLDAN, A.G.S., OLIFF, W.D., ORREN, M.J. & WATLING, R.J. 1983. South African National Scientific Programmes Report No. 73. CSIR. Pretoria. pp. 105.

GLAUERT, A.M., ROGERS, G.E. & GLAUERT, R.H. 1956. A new embedding medium for electron microscopy. *Nature* 178: 803–805

GOLDBERG, E.D., BOWEN, V.T., FARRINGTON, J.W., HARVEY, G., MARTIN, J.H., PARKER, P.L., RISEBROUGH, R.W., ROBERTSON, W., SCHNEIDER, E. & GAMBLE, E. 1987. The mussel watch. *Environ. Conserv.* 5: 101–125.

GOOD, M.W., STOMMEL, E.W. & STEPHENS, R. 1990. Mechanical sensitivity and cell coupling in the ciliated epithelial cells of *Mytilus edulis* gill. *Cell Tissue Res.* 259: 51–60.

GREGORY, M.A. & SPITAELS, J.M. 1987. Variations in the morphology of villous epithelial cells within 8 mm of untreated duodenal ulcers. *J. Path.* 153: 109–119.

HENNIG, H.F.-K.O. 1985. Review of metal concentrations in southern African coastal waters, sediments and organisms. South African National Scientific Programmes Report No. 108. FRD, CSIR. Pretoria. pp. 140.

HIETANEN, B., SUNILA, I. & KRISTOFFERSSON, R. 1988. Toxic effects of zinc on the common mussel *Mytilus edulis* (Bivalvia) in brackish water. II. Accumulation studies. *Ann. Zool. Fennici* 25: 349–352.

HIGASHIYAMA, T., SHIRAISHI, H., OTSUKI, A. & HASHIMOTO, S. 1991. Concentrations of organotin compounds in blue mussels from the wharves of Tokyo Bay. *Marine Pollution Bulletin* 22: 585–587.

JONES, H.D., RICHARDS, O.G. & HUTCHINSON, S. 1990. The role of ctenidial abfrontal cilia in water pumping in *Mytilus edulis* L. *J. Exp. Mar. Biol. Ecol.* 143: 15–26.

JONES, H.D., RICHARDS, O.G. & SOUTHERN, T.A. 1992. Gill dimensions, water pumping rate and body size in the mussel *Mytilus edulis* L. *J. Exp. Mar. Biol. Ecol.* 155: 213–237.

LePENNEC, M., BENINGER, P.G. & HERRY, A. 1988. New observations of the gills of *Placopecten magellanicus* (Mollusca: Bivalvia) and implications for nutrition. II: Internal anatomy and micro-anatomy. *Mar. Biol.* 98: 229–237.

MARTIN, M. & RICHARDSON, B.J. 1991. Long term contaminant biomonitoring: views from southern and northern hemisphere perspectives. *Marine Pollution Bulletin* 22: 533–537.

MURRAY, A.P., RICHARDSON, B.J. & GIBBS, C.F. 1991. Bioconcentration factors for petroleum hydrocarbons, PAHs, LABs and biogenic hydrocarbons in the blue mussel. *Marine Pollution Bulletin* 22: 595–603.

NARBONNE, J.F., GARRIGUES, P., RIBERA, D., RAOUX, C., MATHIEU, A., LEMAIRE, P., SALAUN, J.P. & LAFAURIE, M. 1991. Mixed function oxygenase enzymes as tools for pollution monitoring: field studies on the French coast of the Mediterranean Sea. *Comp. Biochem. Physiol.* 100C: 37–42.

OWEN, G. 1978. Classification of the bivalve gill. *Phil. Trans. R. Soc. Lond.* B. 284: 377–385.

PAVICIC, J., RASPOR, B. & BRANICA, M. 1991. Metal binding proteins of *Mytilus galloprovincialis*, similar to metallothioneins, as a potential indicator of metal pollution. Proceedings of the FAO/UNEP/IOC Workshop on the Biological Effects of Pollutants on Marine Organisms, Valletta (Malta), 10–14 September 1991.

REYNOLDS, E.S. 1962. The use of lead citrate at high pH as an electron opaque stain in electron microscopy. *J. Cell Biol.* 17: 208–212.

RICHARDSON, B.J., GARNHAM, J.S. & FABRIS, J.G. 1994. Trace metal concentrations in mussels (*Mytilus edulis planulatus* L.) transplanted into southern Australian waters. *Marine Pollution Bulletin* 28: 392–396.

RICE, E.L. 1908. Gill development in *Mytilus*. *Biol. Bull.* 14: 61–77.

RIDGEWOOD, W.G. 1903. On the structure of the gills of Lamellibranchia. *Phil. Trans. R. Soc. Lond.*B. 195: 147–284.

SPURR, A.R. 1969. A low viscosity epoxy resin embedding medium for electron microscopy. *J. Ultrastruct. Res.* 26: 31–34.

STEPHENS, R.E. & GOOD, M.J. 1990. Filipin-sterol complexes in molluscan gill ciliated epithelial membranes: intercalation into ciliary necklaces and induction of gap junctional particle arrays. *Cell Tissue Res.* 262: 301–306.

SUNILA, I. 1986. Chronic histopathological effects of shortterm copper and cadmium exposure on the gill of the mussel, *Mytilus edulis*. *Journal of Invertebrate Pathology* 47: 125–142.

SUNILA, I. 1987. Histopathology of mussels (*Mytilus edulis* L.) from the Tvarminne area, the Gulf of Finland (Baltic Sea). *Ann. Zool. Fennici* 24: 55–69.

SUNILA, I. 1988. Pollution-related histopathological changes in the mussel *Mytilus edulis* L. in the Baltic Sea. *Marine Environmental Research* 24: 277–280.

TANABE, S. 1994. International mussel watch in Asia-Pacific phase. *Marine Pollution Bulletin* 28: 518.

TAVARES, T.M., ROCHA, V.C., PORTE, C., BARCELO, D. & ALBAIGES, J. 1988. Application of the mussel watch concept in studies of hydrocarbons, PCBs and DDT in the Brazilian Bay of Todos os Santos (Bahia). *Marine Pollution Bulletin* 19: 575–578.

WINSTON, G.W., MOORE, M.N., STRAATSBURG, I. & KIRCHIN, M.A. 1991. Decreased stability of digestive gland lysosomes from the common mussel *Mytilus edulis* L. by in vitro generation of oxygenfree radicals. *Arch. Environ. Contam. Toxicol.* 21: 401–408.

WRISBERG, M.N. & RHEMREV, R. 1992. Detection of genotoxins in the aquatic environment with the mussel *Mytilus edulis*. Proceedings of the IAWPRC International Symposium, Otsu City (Japan), 25–28 November 1991.